New Findings for the Composition and Structure of Ni Nanoparticles Protected with Organomercaptan Molecules

Matías F. Calderón,[†] Eugenia Zelaya,[‡] Guillermo A. Benitez,[†] Patricia L. Schilardi,[†] Alberto Hernández Creus,[§] Alejandro González Orive,[§] Roberto C. Salvarezza,[†] and Francisco J. Ibañez*,[†]

[†]Instituto de Investigaciones Fisicoquímicas Teóricas y Aplicadas (INIFTA), Universidad Nacional de la Plata, CONICET, Sucursal 4 Casilla de Correo 16 (1900) La Plata, Argentina

[‡]Centro Atómico Bariloche, Comisión Nacional de Energía Atómica-CONICET, Av. Bustillo 9500, 8400 S. C. de Bariloche, Río Negro, Argentina

[§]Departamento de Química Física, Instituto de Materiales y Nanotecnología, Universidad de La Laguna, Av. Astrofísico Francisco Sánchez S/N, La Laguna 38071, Tenerife, Spain

Ⓢ *Supporting Information*

ABSTRACT: Here we explore the synthesis of alkanethiol-coated Ni NPs following the one-phase reaction method by Brust et al.[1] The reduction of $NiCl_2$ with $NaBH_4$ in the presence of dodecanethiol ($C_{12}SH$) yields a complex product that is difficult to identify as illustrated in the figure of merit. We synthesized Ni(II) dodecanethiolate ($C_{12}S$) (without the addition of $NaBH_4$) for comparison and performed an exhaustive characterization with TEM, HR-TEM, AFM, MFM, XPS, XRD, UV−vis, magnetism, and FT-IR. It is found that the organic coating is not quite a well-organized self-assembled monolayer (SAM) surrounding the Ni cluster as previously reported.[2,3] XPS and XRD data show slight differences between both syntheses; however, Ni(II) thiolate appears to be more stable than reduced Ni when exposed to ambient air, indicating the propensity of metallic Ni to oxidize. It has been shown that irradiating with TEM electrons over various metal thiolates leads to nanoparticle formation.[4] We irradiated over Ni(II) thiolate and observed no evidence of NP formation whereas irradiating a reduced Ni sample exhibited an ∼3.0 nm nanoparticle diameter. Magnetism studies showed a difference between both samples, indicating ferromagnetic character for the reduced Ni sample. According to our results, the product of the synthesis is comprised of ultrasmall metallic clusters embedded in some form of Ni(II) $C_{12}S$. In this work, we open a discussion of the chemical nature of the core and the shell in the synthesis of Ni NPs protected with organomercaptan molecules.

Ni(II) Thiolate   Reduced Ni   Dodecanethiol
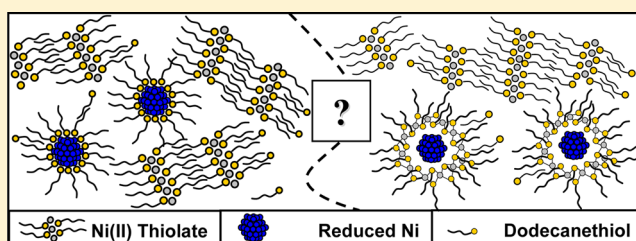
■ INTRODUCTION

The synthesis of chemically modified nanoparticles (NPs) continues to be an exciting topic of research considering its wide range of applications in the field of nanotechnology. Ni is an attractive material because of its relatively low cost and broad range of applications including catalysis,[5] sensing,[6] and spintronics.[7] The versatile Brust-Schiffrin synthesis allows one to obtain metal NPs of controlled sized and composition to tailor functionality through the organic groups and to store the product as a chemical reagent. Although Au is probably the most studied metal because of its inertness and well-known chemistry with organic-containing self-assembled monolayers (SAMs),[8−10] there still remain some concerns about the actual role of reactants and intermediates of synthesis during the reaction. Recently, Lennox[11] and our group[12] began a discussion of the one- and two-phase Brust-Schiffrin synthesis. The former group demonstrated that the surfactant (tetraoctylammonium bromide, TOABr) not only acted as transfer agent but also served as a precursor in the two-phase Brust-Schiffrin reaction whereas the latter group showed that mercaptosuccinic

acid (MSA)-coated Au NPs synthesis yielded small Au NPs coated with an Au(I) alkanethiolate shell. Leff et al.[13] assembled primary amines on Au NPs and determined that a much larger concentration (molar ratio) of amines to Au (∼11:1) was required as compared to conventional alkanethiol-coated Au MPC. Eklund and Cliffel explored other metals and demonstrated the need to use a stronger reducing agent (lithium triethylborohydride) in place of $NaBH_4$ for the synthesis of stable alkanethiol-coated Pt NPs.[14] Since these new inputs and others,[15,16] researchers have been encouraged to explore more in depth the actual chemistry evolved during the Brust synthesis. Some examples include the use of X-ray adsorption spectroscopy (XAFS)[17] and kinetic studies of the nanoparticle size evolution,[18] the actual role of the surfactant-forming micelles,[19] and the implications of intermediates[20] such as Te, Au, and Ag, just to mention a few.

The synthesis of less noble and catalytically active metal NPs such as Pd,[16,21,22] Ni,[2,3,23] and Ag[24] brings about new challenges in research because of their propensity to oxidize and the potential formation of unexpected intermediates or products. Moreover, if the metal precursor has magnetic properties (i.e., Ni, Fe, and Co), then aggregation due to magnetic interactions between NPs may occur. In the case of alkanethiols on Pd, Murray and co-workers[16] first demonstrated that the synthesis of Pd monolayer-protected clusters (MPCs) was sensitive to the thiol/Pd molar ratio. They observed that thiol/Pd ≤ (1:1) leads to metallic Pd(0) whereas ≥ (2:1) yielded a more complex material supposedly comprised of small metallic clusters protected by some form of Pd(II) alkanethiolate. Another example may include the work of Zamborini and co-workers,[25] who unexpectedly found that as-prepared alkylamine-coated Pd MPCs yielded to some form of alkyl nitriles as evidenced in FT-IR experiments. Surprisingly, the peak at 2167 cm^{-1} assigned to nitriles disappeared during H$_2$ sensing applications. Later, Corthey et al.[21] following the study performed by alkanethiols SAMs on Pd thin films[26] and amine-coated Pd NPs place-exchanged with alkanethiolates[22] confirmed the formation of a Pd sulfide (PdS) submonolayer in the synthesis of alkanethiolate-coated Pd MPCs. The former examples evidenced the formation of new compounds (intermediates or products) during the Brust-Schiffrin synthesis, which requires close attention regardless of the implications that it may hold for the applied field.

Organic-coated Ni NPs have been synthesized using microemulsion techniques,[27] laser decomposition,[28] or the reduction of metal ions in the presence of various ligands including dendrimers,[29] alkylamines,[30] alkanethiols,[2,3] polymers,[23] and surfactants.[31] The organic ligands passivate the surface of the growing NPs controlling its diameter and providing stability. However, the majority of the above synthesis yielded to large NP diameter likely because of difficulties in preventing NiO formation. Crooks and co-workers[29] successfully synthesized Ni NPs by reducing Ni ions inside dendrimers and obtained NPs with diameters smaller than 4 nm. Others have synthesized Ni/Au[32] and Ni/Fe[33] alloy NPs coated with different dendrimer generations. Recently, Wu and co-workers synthesized three generations of phosphine-coated Ni NPs for further use in Suzuki coupling reactions.[34] The synthesis of Ni nanorods in the presence of hexadecyl-amine (HDA) or trioctylphosphine oxide (TOPO) has been performed and has been proven to have magnetism.[35] Legrand et al.[36] reduced Ni(II) ions with NaBH$_4$ in the presence of inverse micelles (sodium bis (2-ethyl-hexyl) sulfosuccinate, AOT) and characterized the formation of Ni$_2$B NPs by means of XPS. Surprisingly, the synthesis and characterization of organomercaptan-coated Ni NPs have been scarcely explored or incompletely characterized.[2,3] Bai and co-workers[2] were probably the first to report the reduction of Ni salt in the presence of dodecanethiol (C$_{12}$SH). Later, Wan and co-workers[3] synthesized Ni NPs in the absence and presence of dodecanethiol-protected ligands with the use of hydrazine hydroxide. Glavee et al.[37] studied mechanistic and stoichiometric issues for the reduction of Cu(II) and Ni(II) ions with NaBH$_4$ in aqueous and nonaqueous (using diglyme) solutions. A few groups assembled alkanethiols of various lengths on mechanically polished,[38] sputtered,[39] chemically reduced,[40] or electrodeposited[41] Ni thin films. The difference between their approach and ours relies on the fact that alkanethiol SAMs usually chemisorb on a pretreated film in the absence of any intermediate of synthesis.

Our initial goal was to use organic-coated Ni NPs in H$_2$ sensing applications. Ni has been demonstrated to be an excellent material for H$_2$ sensing because, when alloyed with Pd, it suppresses intermediate $\alpha-\beta$ formation[42] without suffering structural changes after repeated H$_2$ cycles,[43] leading to a faster and more stable sensor. However, it is well known that sulfur-containing compounds poison the metal catalyst, diminishing its sensing activity.[22] It is also demonstrated that long alkyl chains may prevent the metal−hydrogen interaction.[25] We failed in the attempt to synthesize short alkylamine- and surfactant-coated Ni NPs following various synthesis protocols. Table S1 in the Supporting Information describes some of the synthesis performed before the actual synthesis shown in this work.

Here, we report the synthesis and characterization of Ni NPs and Ni(II) thiolate, Ni(II) C$_{12}$S following the one-phase reaction method by the Brust-Schiffrin protocol. The metal salt (NiCl$_2$) dissolved in anhydrous ethanol was reduced with NaBH$_4$ in the presence of 1-dodecanethiol. The solution changed color from green to brown after the addition of the protecting ligands and finally turned darker brown when reduced with NaBH$_4$. An exhaustive characterization proves that the product of synthesis cannot be simply described as a monolayer-protected Ni cluster. It is rather a complex material comprised of some form of Ni(II) C$_{12}$S polymer in coexistence with ultrasmall Ni clusters.

■ EXPERIMENTAL SECTION

Chemicals. Sodium borohydride (96%), toluene (99.8%) for HPLC, and ethanol anhydrous (99.8%) plus for HPLC were purchased from Aldrich Chemical Co., ACS-grade methanol (99.8%) and acetonitrile (99.9%) HPLC/Spectro were purchased from Tedia, n-hexane (99.3%) was purchased from Anedra S. A., NiCl$_2$ (98%) was purchased from Analar, 1-dodecanethiol (98%) was purchased from Aldrich, and Milli-Q water (17.8 MΩ cm) was employed for all aqueous solutions. All reactions were conducted under ambient conditions.

Synthesis. *Synthesis of Ni/C$_{12}$SH (1:1).* Ni NPs were synthesized by taking 10 mL of NiCl$_2$ (0.02 M) in ethanol, and 48 μL (0.2 mmol) of pure 1-dodecanethiol (C$_{12}$SH) was added to the solution. Later, 2 mmol of NaBH$_4$ dissolved in 5 mL of Milli-Q water was added, leading to an instant color change from green to dark brown accompanied by gas evolution. The reaction was allowed to proceed until no gas was observed. Then, toluene was added in order to transfer the NPs to the organic phase, agitation was turned off, and the phases were separated. The product was purified by precipitation with absolute ethanol, centrifuged, and redispersed. This procedure was repeated at least three times. The product obtained was stored in toluene and kept at low temperature (−4 °C ≤ T < 0 °C). The general reaction scheme for the reduction of Ni ions is shown below:

$$2Ni^{+2}_{(EtOH)} + 4BH^{-}_{4(ac)} + 10.5H_2O + 0.75O_2$$
$$\rightarrow 2Ni^0 + 4B(OH)_3 + 12.5H_{2(g)}$$
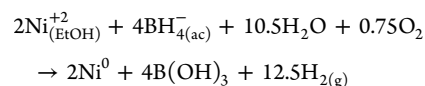
Synthesis of Ni(II) Dodecanethiolate. Ni(II) dodecanethiolate (C$_{12}$S) was synthesized in the same manner as Ni NPs but without the addition of NaBH$_4$. Briefly, 96 μL of pure C$_{12}$SH (0.4 mmol) was added to NiCl$_2$ (10 mL, 0.02 M) dissolved in ethanol, followed by the addition of 4 mL of 0.1 M NaOH (0.4 mmol). The reaction was allowed to proceed until all thiolates precipitated. The product was purified following the same procedure as for reduced Ni synthesis.

Synthesis of Au C$_{12}$S MPCs. It was synthesized following the Brust-Schiffrin method.[1]

Spectroscopy. X-ray Photon–Electron Spectroscopy (XPS). The samples were characterized by XPS using a Mg Kα source (XR50, Specs GmbH) and a hemispherical electron energy analyzer (PHOIBOS 100, Specs GmbH). Samples were dispersed in toluene followed by drop-cast deposition onto different substrates. Various substrates were employed, including oriented Si, Si wafers covered with sputtered Cr/Au (Si/SiOx/Cr/Au), and spectroscopically pure vitreous carbon discs (Ted Pella, Inc.). Silicon substrates were treated with piranha solution and thoroughly rinsed with nanopure water and dried under an N_2 gun. (*Caution! Piranha solution can react violently with organic matter.*)

UV−Vis. UV–visible spectroscopy (UV−vis) was performed with a Perkin-Elmer Lambda 35 spectrometer equipped with a double beam. The sample dispersed in toluene was placed in a quartz cuvette for UV−vis measurements. Because of the interference of the organic solvent, the plot was run between 300 and 900 nm.

Fourier Transform Infrared (FT-IR). FT-IR measurements were acquired on a PIKE Miracle Varian 600 instrument in transmission mode by drop-casting the product of synthesis onto clean glass slides. Once the solvent was evaporated, transmission FT-IR samples were run under ambient conditions.

Powder X-ray Diffraction (XRD). X-ray diffraction measurements were acquired with Cu Kα radiation (λ = 1.5406 Å) using a Phillips PW-1710 diffractometer with monochromatic radiation under Bragg−Brentano geometry. An X-ray diffraction spectrum was acquired under ambient conditions in the angle range from 2 to 100° with a step size of 0.02° every 15 s. Samples were placed on nonabsorptive glass in the form of fine powder or drop-cast deposited from toluene dispersions.

Magnetism. Magnetic studies were carried out on an AC Susceptometer LakeShore 7130. Each susceptibility measurement (χ) was taken as an average (avg χ) value after the temperature of the system became stable. We employed a temperature range from 18.6 to 323 K run at 825 Hz, Hac = 1 Oe, Hdc = 0 Oe. M−H plots were obtained from a vibrating sample magnetometer (VSM) LakeShore 7404 run at 26 °C from a −1.9 to 1.9 T magnetic field.

Microscopy. *Transmission Electron Microscopy (TEM) and High-Resolution Transmission Electron Microscopy (HR-TEM).* Samples were drop-cast onto ultrathin carbon films over Cu TEM grids, and images were acquired using a FEI CM200 UT operated at 200 keV.

Atomic Force Microscopy (AFM) and Magnetic Force Microscopy (MFM). Samples were drop-cast onto highly oriented pyrolytic graphite (HOPG). Magnetic force gradient (MFM) and topographic images were acquired with a NanoScope V scanning probe microscope (Bruker) run under ambient conditions. Lift heights ranging from 5 to 25 nm were used for the measurements. Images were taken at 1 Hz using a magnetic MESP (60−100 kHz, 1−5 N/m) scanning probe coated with a magnetic Co/Cr alloy thin film. Silicon FESP tips with the same range of frequency, force constant, and dimensions were used to compare the contrast phase signal obtained with both tips at different sample heights. Prior to acquiring MFM images, the tips were exposed to a 0.3 T magnetic field.

RESULTS AND DISCUSSION

Shell. Figure 1A shows a selected transmission electron microscopy (TEM) image of as-synthesized Ni NPs along with an enlarged image of an individual nanoparticle. Figure S1 (Supporting Information) shows more TEM images along with a histogram corresponding to a 3.16 ± 0.5 nm average diameter. The enlarged image in Figure 1A clearly shows a well-defined "halo" or shell surrounding a Ni core attributed to graphitic or amorphous carbon.[44] Similar TEM images have been shown for nickel boride (Ni_2B) NPs whose core−shell structure is clearly observable.[36] Williams and co-workers also demonstrated the formation of core−shell structures with filled and voided interiors caused by TEM irradiation on amorphous metal oxides.[45] We performed several different kinds of synthesis (Table S1) employing different Ni/thiol molar ratios and found that a molar ratio of <1 led to NP aggregation.

as-synthesized (Reduced Ni)
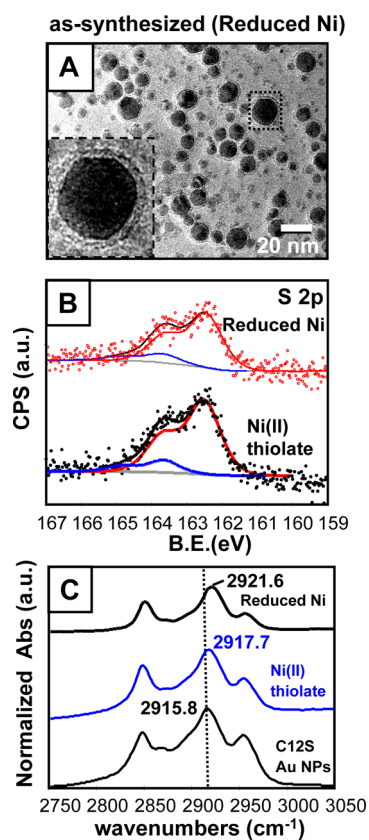
Figure 1. TEM image of as-deposited reduced Ni NPs (A), XPS spectra in the S 2p region (B), and FT-IR plot for $C_{12}S$ Au MPCs (C), showing as-synthesized reduced Ni and Ni(II) dodecanethiolate ($C_{12}S$) samples. XPS and FT-IR plots are offset for better comparison.

The data shown in Figure 1B,C have something in common: there is no distinct difference between plots for reduced Ni (with $NaBH_4$) and Ni(II) dodecanethiolate (no $NaBH_4$). As an example, XPS in Figure 1B shows no noticeable difference between reduced Ni and Ni(II) $C_{12}S$, indicating that it is difficult to distinguish between sulfur species in the synthesis. A closer inspection of the fitting of the S 2p region shows two peaks at low 162.5 eV and high 163.6 eV binding energies attributed to thiolate and other species (i.e., free thiol), respectively. The percent ratio between thiolate and free thiol corresponds to 86 to 14%, respectively. However, the ratio Ni/S corresponds to 1.0:2.1, which is higher than the stoichiometry used in the synthesis. The excess S observed in XPS with respect to the concentration used in the synthesis indicates excess sulfur-containing species, which may include Ni(II) $C_{12}S$, chemisorbed $C_{12}SH$, physisorbed $C_{12}SH$, and Ni sulfide (NiS). Because Ni is a catalytically active metal, it is reasonable to expect the formation of NiS as recently demonstrated for alkanethiols on Pd films[26] and on Pd NPs.[21] Unfortunately, it is difficult to assign an NiS peak because the S 2p peak may appear somewhere in between 161.0 and 162.2 eV, overlapping the actual (~162.5 eV) S 2p thiolate peak.

Vibrational spectroscopy in Figure 1C provides important information about the order and conformation of the organic alkane chains assembled on a surface.[10,46,47] Accordingly, we performed FT-IR experiments to gain insights into the alkane chain order (i.e., gauche defects) by looking at changes in the asymmetric ($d^−$) CH_2 stretching vibrations. Figure 1C shows a comparison between dodecanethiolate Au monolayer-protected

clusters, $C_{12}S$ on Au MPCs (used as a model) with Ni(II) $C_{12}S$ and $C_{12}S$ on reduced Ni. The alkane chain organization follows the order $C_{12}S$ Au MPCs (2915.8 cm^{-1}) > Ni(II) $C_{12}S$ (2917.7 cm^{-1}) > $C_{12}S$ on reduced Ni (2921.6 cm^{-1}) > neat $C_{12}SH$ (2925 cm^{-1}).[48] As expected, neat thiols (2925 cm^{-1}) were more disorganized (at higher frequency or energy) than $C_{12}S$ on reduced Ni whereas the Ni(II) $C_{12}S$ peak (2917.7 cm^{-1}) exhibited the highest order among Ni compounds. Alkanethiols usually chemisorb on metal surfaces in a well-organized and packed arrangement caused by the strong coordination of thiols to the surface accompanied by van der Waals interactions between hydrocarbon tails. It has been proven, for instance, that the longer the alkane chain the lower the gauche defects indicated by a shift of the C–H stretching vibrations toward lower wavenumbers.[47] Our group recently demonstrated the influence of polar and nonpolar vapors on the shifting of (d$^-$) CH$_2$ stretching vibrations of a surfactant-coated Au NP film.[46] Surprisingly, the wavenumber reported in the literature for Ni NPs reduced with hydrazine[3] falls within the value of our Ni(II) thiolate peak (2917.7 cm^{-1}), indicating order for both compounds despite their different chemistry. Our FT-IR result for Ni(II) thiolate is consistent with the formation of a recently reported crystalline structure,[48] with AFM images (Figure S2) where clusters of thiolates can be clearly seen, and finally with our XRD experiments (vide infra). According to our results, we cannot define the organic coating for reduced Ni as a well-organized alkanethiolate monolayer protecting a Ni cluster.

Core. Now we turn to a discussion of the chemical nature of the core. Figure 2A shows XPS region for Ni 2p$_{3/2}$ from an as-synthesized reduced Ni sample whose profile indicates metallic character with no signs of oxidation. Our data are consistent with octanethiol SAMs chemisorbed on pretreated Ni films including those obtained by sputtering under high-vacuum conditions[39] or by electrochemically reducing Ni oxide.[41]
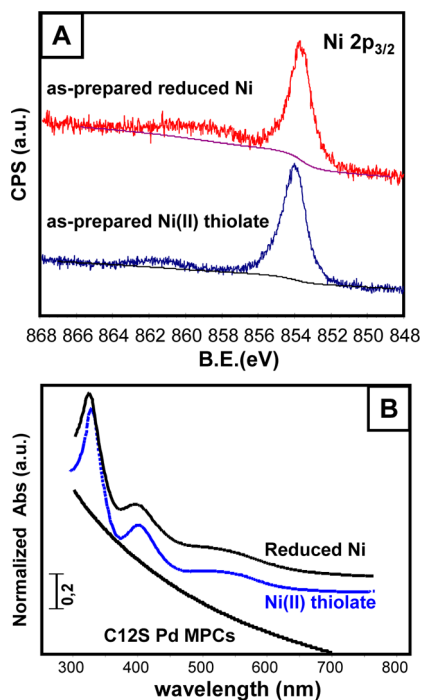
However, reported benchtop synthesis performed for dodec-anethiol-coated Ni NPs exhibited oxidation.[3] It was speculated that NP oxidation took place either during the synthesis (reducing with hydrazine hydroxide) or later during sample manipulation in air. At first glance, our XPS data may seem relevant because we obtained metallic Ni, with no signs of oxidation, via a simple benchtop synthesis. Nevertheless, XPS for Ni(II) thiolate exhibits similar profiles to the sample reduced with NaBH$_4$. In summary, XPS provides information about the presence or absence of oxides on the Ni surface but cannot discriminate between zero-valent Ni and Ni(II) in Ni(II) $C_{12}S$ samples.

The UV–vis plot in Figure 2B again shows no distinct difference between reduced Ni and Ni(II) $C_{12}S$. Transition-metal NPs such as Pt, Pd, and Ni usually scatter light (no plasmon or absorbance) in the UV–vis range similarly to $C_{12}S$ Pd MPCs used as comparison in Figure 2B. Here, both Ni syntheses show three absorbance peaks at ∼522, ∼412, and ∼336 nm consistent with those observed in the literature for Ni(II) butanethiolate[49] and Pd(II) hexanethiolate[16] and attributed to metal-to-ligand and ligand-to-metal charge-transfer bands. It is clear from the figure that UV–vis profiles for Ni species are similar between them but different when compared to metallic Pd MPCs. To the best of our knowledge, reports that claimed to obtain alkanethiol-coated Ni NPs[2,3] have not shown profiles characteristic of metallic Ni. At this point, UV–vis data indicate the presence of some form of Ni(II) $C_{12}S$ with profiles different from those of transition-metal NPs (i.e., Pd). These data impart some degree of complexity, driving us to the use of other characterizations techniques.

Microscopy data in Figure 3A and Figure 3B–D show AFM and TEM images of as-synthesized reduced Ni drop-coated on highly oriented pyrolytic graphite (HOPG) and reduced Ni and Ni(II) thiolate deposited on a TEM grid, respectively. The selected AFM image shows some aggregates along with the film height range between 0.7 and 3.6 nm obtained by the cross sections shown next to the figure. Figure S2 shows more AFM images. The selected TEM image shown in Figure 3B exhibits NPs polydispersity with one prominent size population corresponding to ∼3.2 nm (vide supra) and two other secondary populations with ∼2 and ∼4 nm diameters as described by the histogram in Figure S1. Interestingly, it also shows small rings pointed out with arrows and depicted with numbers next to the main figure. Figure 3C shows high-resolution TEM image of a larger (∼6 nm) individual nanoparticle with a (110) crystalline domain surrounded by a well-defined shell. Figure S3 shows interesting TEM and HR-TEM images exhibiting atomic row dislocations within a single nanoparticle. Finally, Figure 3D shows a TEM image taken after 1 h of irradiation over Ni(II) thiolate previously deposited on a Cu grid. Next to the figure, an Electron Diffraction Spectroscopy (EDS) plot confirms the presence of Ni and S from the sample and Cu from the grid.

If we consider a small Ni core surrounded by a well-ordered alkanethiol monolayer, then the height of the nanoparticle measured by AFM should be ∼4 nm (∼3 nm accounted for by the dodecanethiol shell plus an ∼1-nm-diameter cluster), which falls a little above the upper height range obtained by AFM in Figure 3A. The different film heights measured in AFM may be in line with the organic chain disorder observed through FT-IR experiments, making it difficult to predict the structure or morphology adopted by the organic material (thiolate) after
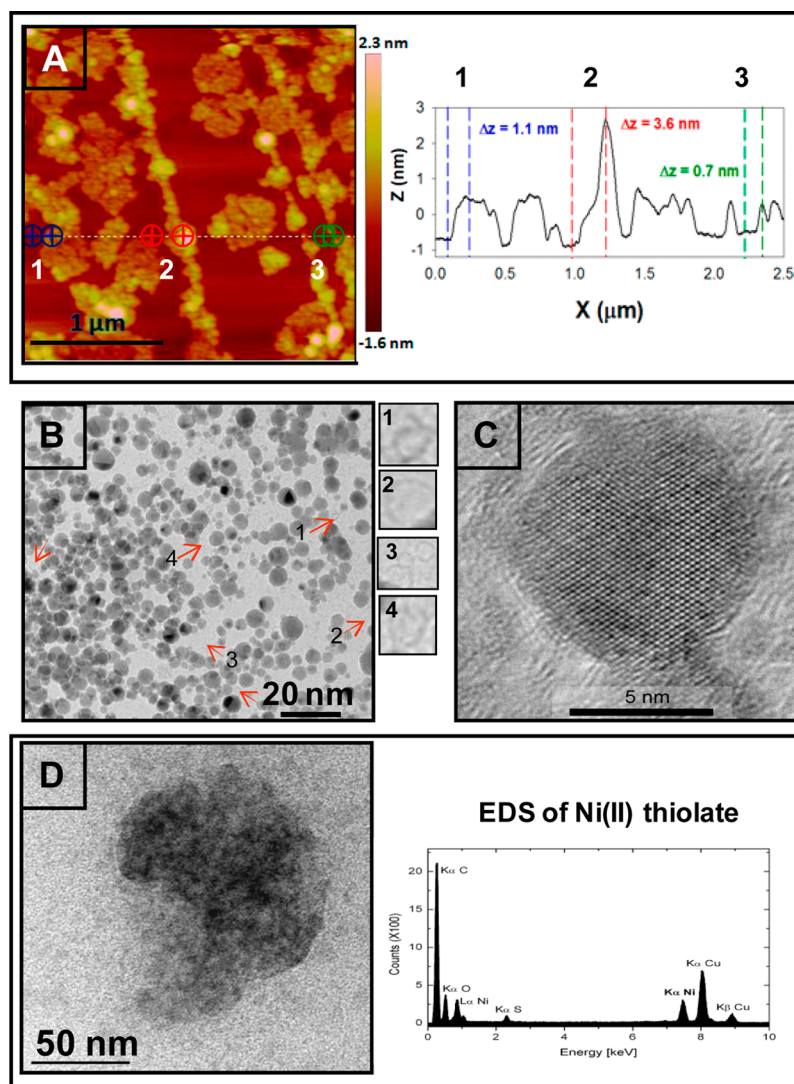

Figure 2. XPS spectra for Ni 2p$_{3/2}$ (A) and UV–vis plot for $C_{12}S$ Pd MPCs (B) showing as-synthesized reduced Ni (A) and Ni(II) $C_{12}S$. UV–vis profiles are offset for better comparison.

Figure 3. AFM image along with cross sections taken in three different regions (A), TEM image with arrows pointing to ringlike structures (B), and HR-TEM image of a single nanoparticle of as-deposited reduced Ni synthesis (C). A TEM image of Ni(II) thiolate along with an EDS plot after a long irradiation time (D).
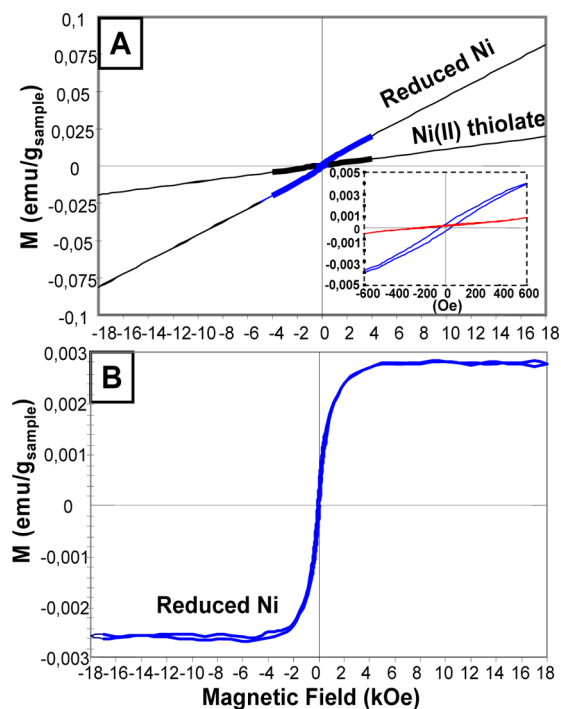
reduction with $NaBH_4$. On the contrary, AFM images of Ni(II) thiolate exhibited an overall constant ~2.3 nm average film height obtained from various cross-section (Figure S2). It has been shown that thiolates form well-defined and ordered crystalline structures[49,50] consistent with the FT-IR (vide supra) and XRD results discussed below. From the above results, we assume that the wide cross-section range observed in AFM along with ring structures observed in TEM indicates the presence of some form of Ni(II) $C_{12}S$ (~2.3 nm average height value) in coexistence with a dodecanethiolate-capped ultrasmall Ni core[29] (upper height value in AFM for reduced Ni).

Figure 3B shows a TEM image for as-deposited reduced Ni, which exhibits larger NPs than AFM (assuming the existence of a small metallic core of ~1−1.5 nm diameter). Figure 3B shows two interesting aspects. First, it is likely that there are two other size populations corresponding to ~2 and ~4 nm diameter. Second, there are small, hollow ring-shaped structures. The relatively larger NP diameter seen in TEM could be attributed to electron irradiation while acquiring the image. Accordingly, Figure 3C shows the HR-TEM image of an individual nanoparticle that is 2 times larger (~6 nm) than the actual

average diameter. It has recently been demonstrated that TEM irradiation over Au(I) octadecanethiolate led to NPs nucleation and growth with sizes ranging from 2 to 5 nm diameter depending on the TEM accelerating voltage.[4] In their work, they demonstrated (a) new nucleation centers of ~2 nm diameter were formed by in situ reducing thiolate at high irradiating voltage (200 KeV) and (b) from those clusters larger NPs (~5 nm) were eventually grown. That report clarified the usual discrepancy about nanoparticle size observed between TEM and other techniques.[10,51,52] For instance, it has been determined that there were two different diameters for thiomalate-coated Au NPs: ~1.0 and 3.5 nm depending on the characterization technique used.[12] In their work, they indicated that alkanethiolated polymer surrounding a small Au nanoparticle (~1 nm) increased its size by more than a factor of ~3 from an initial measurement by small-angle X-ray scattering (SAXS) toward larger NPs observed by HR-TEM. As a control experiment, we exposed as-synthesized Ni(II) $C_{12}S$ to 200 keV and observed no NP formation as indicated in Figure 3D. Our results differ from the above report,[4] where Au(I) alkanethiolates evolved to Au NPs and grew under TEM

irradiation. Furthermore, Kulkarni and co-workers obtained nanoparticle patterns by irradiating over numerous different metal ion complexes including Au, Pt, Pd, Ag, Pb, and Cu but surprisingly not Ni.[53] Our results may shed light on the importance of the metal composition and its role during the in situ reduction of metal ions. In summary, the presence of well-defined and crystalline NPs observed by TEM may indicate that ultrasmall Ni NPs are needed for further NPs growth. The large polydispersity and high irradiating energy used in our TEM (200 keV) is consistent with the small NPs that are formed (1 to 2 nm), which grew further to different extents, either ~3.2 or 4−6 nm. Others have synthesized Ni_2B NPs under anaerobic conditions and discussed their stability when using TEM as a result of severe structural changes.[36] Therefore, the presence of small ring-shaped structures could be caused by strong TEM irradiation. We also observed astigmatism in TEM experiments for reduced Ni samples and attributed this to the magnetic properties of Ni. By means of magnetic force microscopy (MFM) we corroborated the existence of magnetism in reduced Ni NPs (Figure S4).

Further magnetic studies were conducted using magnetrometry for both samples involved in this work. Figure S5 shows a field-cooled magnetization analysis for reduced Ni and Ni(II) thiolate run from 18.6 to 323 K. The plot also shows a Curie−Weiss temperature of ~+25 K for the reduced Ni sample, where the positive sign indicates the ferromagnetic interaction between spins. Figure 4A,B shows room-temperature magnet-
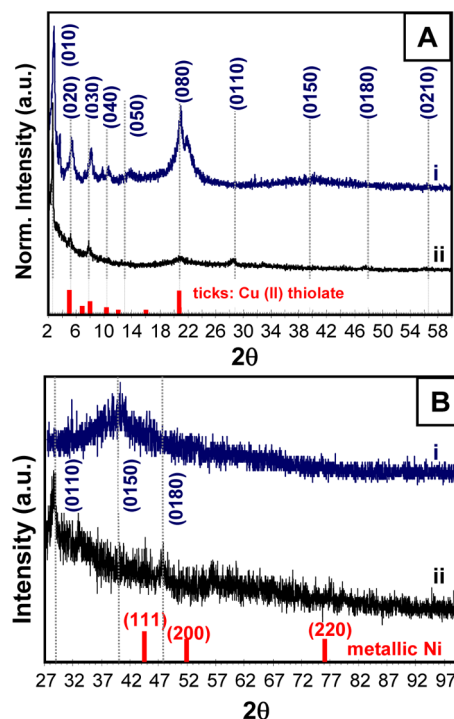
ferromagnetic contribution from the reduced Ni sample with corresponding magnetic saturation (Ms) and coercivity (Hc) values of 2.5×10^{-3} emu/g of sample and 40 Oe, respectively. It is known that the magnetic properties are dependent on the size of the magnetic materials and how this is affected by the thermal energy. It has been demonstrated that magnetic saturation in nanomaterials occurs at lower values than for their counterparts (bulk materials).[54] For instance, bulk Ni and Ni NPs with 4.6 nm diameter exhibited saturation magnetization values of 55[54] and 26.2 emu/g,[55] respectively. Others observed even lower magnetization values for smaller NPs corresponding to 10 emu/g[32] of Ni and 3.4 emu/g[29] of Ni for 3.0 nm NiAu alloyed NPs and an ~0.8 nm Ni NP diameter (comprised of ≥140 atoms), respectively, run at 5 K. Surprisingly, our magnetic saturation value (~2.5×10^{-3} emu/g) is almost 3 orders of magnitude smaller than that reported for dendrimer-coated Ni NPs.[29] It is worth noticing that both syntheses of NPs resemble each other because they are comprised of minority Ni centers surrounded by a vast majority of polymer (dendrimers or alkanethiolates). The key difference, though, relies on the fact that our experiments were run at 295 K higher temperature and magnetization values were expressed in grams of sample, resulting in a significantly lower magnetic susceptibility. Importantly, our results showed some difference between both samples, indicating ferromagnetic behavior for reduced Ni consistent with the higher magnetic susceptibility shown in Figure S5. These data again support the presence of ultrasmall Ni NPs with ferromagnetic properties at room temperature. Ni(II) thiolate exhibited paramagnetic properties over the entire magnetization field.

Figure 5 shows XRD data for reduced Ni and Ni(II) $C_{12}S$. There are more similarities than differences between both

Figure 4. M−H plots run at 25 °C over the indicated magnetic field for both samples (A) and for reduced Ni with a subtracted background (B). The inset shows M−H loops at low magnetic field.

Figure 5. XRD spectra at low angles (A) and high angles (B) for Ni(II) $C_{12}S$ (i) and reduced Ni (ii). The height and position of tick marks at the bottom show assignments reported in the literature as indicated.

ization versus the magnetic field (M−H) loops for both samples and a linear subtracted background for the reduced Ni sample, respectively. Although the profiles and slopes in Figure 4A are similar, the reduced Ni sample exhibited ferromagnetic behavior at low magnetic field as indicated in the inset and Figure 4B. The s-shaped curve in Figure 4B demonstrates the

syntheses. First, XRD at low angles for Ni(II) $C_{12}S$ shows a progression of reflections, which represents the diffraction pattern from a layered structure. This peak periodicity is associated with the interlayer spacing between planes (comprised of S and Ni atoms) separated by dodecanethiolate chains whereas small peaks in between represent intralayer distances. The dotted vertical lines in Figure 5A indicate the reflection patterns for Ni(II) $C_{12}S$, in good agreement with peaks observed for Cu(II) $C_{16}S$ (ticks marks at the bottom of Figure 5A)[56] and Ag(I) $C_{12}S$[57] (not shown here). Sanyal and co-workers[49] proposed a bilayer structure for Ni(II) alkanethiolates of various chain lengths comprised of two fully extended alkanethiolate chains with S and Ni atoms placed in-plane. In their work, they observed that the spacing between reflections increased linearly from ~13 to ~43 Å as the organic chain length increased from 3 to 15 methylene units. In view of their results and on the basis of our calculations, the spacing between reflections corresponds to 33.97 Å, which is close to the value for an ideal bilayer structure (28 Å). (Table S2 and Figure S6 show calculations via the Bragg formula.) Some groups have demonstrated that Pd and Ni complexed with sulfur compounds form stable crownlike structures via a tetra-coordinated metal−ligand interaction.[58,59] Second, note that even at lower intensity, some reflections for reduced Ni match up well with those for Ni(II) $C_{12}S$. In conclusion, as-prepared reduced Ni exhibited 010, 020, 030, and 080 reflections that fit well with those corresponding to Ni(II) $C_{12}S$. It is important to point out that the XRD results for Ni(II) $C_{12}S$ showed well-ordered bilayer structure consistent with the alkane chain order observed in FT-IR experiments (Figure 1C) and constant film height determined by AFM (Figure S2) .

Figure 5B shows no drastic difference between Ni(II) $C_{12}S$ and reduced Ni except for the weak intensity of the latter and the appearance of a large reflection peak at $2\theta = 39$ (0150) for the former. The tick marks depict the crystalline domains along with their intensity (height of the tick) from metallic Ni used as a reference (PDF no. 011260). Interestingly, none of the metallic assignments matched up with peaks observed for the reduced Ni sample. Unfortunately, XRD cannot resolve the presence or absence of crystalline domains for the reduced Ni sample because the signal (peaks) lies within the noise level of the instrument. Therefore, the appearance of weak reflections with no signs of crystalline domains could be consistent with TEM images where we observed hollow ringlike structures. TEM images also showed small and large NP populations for reduced Ni synthesis whereas the irradiation of Ni(II) thiolate caused no nanoparticle formation.

Sample Stability and Postsynthesis Treatments. We studied the effects of sample stability and postsynthesis treatments for as-prepared reduced Ni NPs kept in toluene and as-deposited Ni films exposed to ambient conditions for a week. We believe it is fair to characterize Ni films by XRD, XPS, FT-IR, and AFM because postsynthesis treatments were conducted similarly. For instance, samples used in XRD and FT-IR required the drop-coating of the NPs on a substrate, which involves exposure of the film to air after solvent evaporation. Figure 6A−C shows XPS and XRD plots with apparent differences between as-prepared and aged samples. Figure 6A shows signs of oxidation noticed by the increase in the NiO peak developed at the Ni $2p_{3/2}$ satellite whereas the Ni(II) thiolate sample showed almost no oxidation under the same conditions (Figure 6B). To better prove oxidation, we examined O_2 1s and confirmed oxidation for the reduced Ni
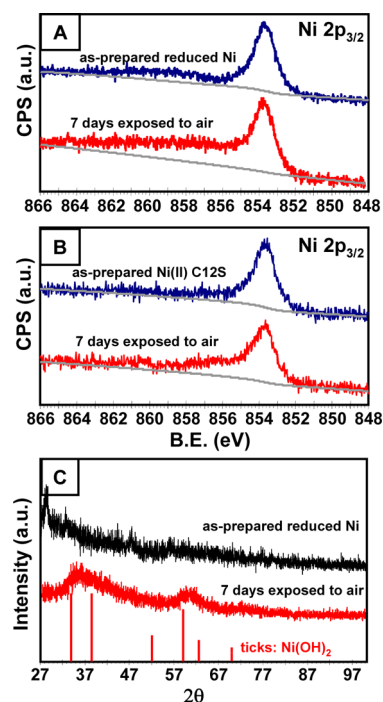
Figure 6. XPS data in the Ni $2p_{3/2}$ region for reduced Ni (A) and the Ni thiolate sample (B) as prepared and after 7 days of exposure to air. XRD plot (C) for as-prepared reduced Ni and after 7 days of exposure to ambient conditions. The height and position of tick marks at the bottom represent assignments for $Ni(OH)_2$ as reported in the literature.

sample (Figure S7). The kinetics of oxidation is shown in Figure S8, indicating quick oxidation for the reduced Ni sample after 12 h of air exposure. Figure 6C shows XRD plots for the oxidation of reduced Ni after 7 days of exposure to air. The XRD plot after air exposure shows two broad, weak peaks near the position of the most intense tick marks assigned in the literature to $Ni(OH)_2$,[60] shown at the bottom of the figure. There is again evidence that the Ni cores may readily reacted with O_2 to form NiO, consistent with XPS results. XPS data in Figure S9 shows good sample stability for as-synthesized and ~2-month-old reduced Ni samples kept in toluene at −2 °C.

■ CONCLUSIONS

We synthesized and fully characterized the synthesis of reduced Ni and Ni(II) $C_{12}S$ following a modified Brust-Schiffrin synthesis. The characterization techniques used in this work exhibited similarities and differences between both products of synthesis. For instance, XPS, UV−vis, and XRD showed no drastic differences between both samples. AFM (cross-section) showed a height range of 0.7 to 3.6 nm whereas TEM exhibited various size populations and hollow ringlike structures. XRD showed reduced Ni with some reflections similar to those of Ni(II) $C_{12}S$ with no signs of metallic domains likely as a result of the small signal-to-noise (S/N) ratio. However, irradiating with TEM on Ni(II) $C_{12}S$ showed no nanoparticle formation, suggesting that large NPs arose from the in situ reduction of Ni(II) thiolate on the surface of metallic Ni cores present in the reduced sample. In addition, XPS and XRD showed oxidation for reduced Ni over 7 days of exposure to ambient conditions attributed to the presence of readily reactive metallic centers. Magnetic studies showed a higher magnetic susceptibility for reduced Ni samples, suggesting the presence of metallic NPs.

From these data, it is feasible to define the product of synthesis as the coexistence between some form of alkanethiolate polymer and an ultrasmall Ni cluster. When reduced Ni synthesis is carried out in an organic solvent, it lasts for long periods of time without signs of oxidation. More experiments including EXAFS will be performed in order to determine the structure of the material better.

■ ASSOCIATED CONTENT

Ⓢ Supporting Information

Additional synthesis routes, TEM and high-resolution TEM of reduced Ni nanoparticles, topographic and magnetic AFM images, XRD calculations, magnetic susceptibility, and XPS data. This material is available free of charge via the Internet at http://pubs.acs.org.

■ AUTHOR INFORMATION

Corresponding Author
*E-mail: fjiban@inifta.unlp.edu.ar.

Notes
The authors declare no competing financial interest.

■ ACKNOWLEDGMENTS

■ REFERENCES

(1) Brust, M.; Walker, M.; Bethell, D.; Schiffrin, D. J.; Whyman, R. Synthesis of Thiol-Derivatised Gold Nanoparticles in a Two-Phase Liquid-Liquid System. *J. Chem. Soc., Chem. Commun.* **1994**, 801.

(2) Lei, S.-B.; Wang, C.; Yin, S.-X.; Wan, L.-J.; Bai, C.-L. Assembling Nanometer Nickel Particles into Ordered Arrays. *ChemPhysChem* **2003**, *4*, 1114−1117.

(3) Chen, L.; Chen, J.; Zhou, H.; Zhang, D.; Wan, H. Synthesis of Dodecanethiol Monolayer-Stabilized Nickel Nanoparticles. *Mater. Sci. Eng., A* **2007**, *452−453*, 262−266.

(4) Kim, J.-U.; Cha, S.-H.; Shin, K.; Jho, J. Y.; Lee, J.-C. Synthesis of Gold Nanoparticles from Gold(I)−Alkanethiolate Complexes with Supramolecular Structures through Electron Beam Irradiation in TEM. *J. Am. Chem. Soc.* **2005**, *127*, 9962−9963.

(5) Park, J.; Kang, E.; Son, S. U.; Park, H. M.; Lee, M. K.; Kim, J.; Kim, K. W.; Noh, H.-J.; Park, J.-H.; Bae, C. J.; Park, J.-G.; Hyeon, T. Monodisperse Nanoparticles of Ni and NiO: Synthesis, Characterization, Self-Assembled Superlattices, and Catalytic Applications in the Suzuki Coupling Reaction. *Adv. Mater.* **2005**, *17*, 429−434.

(6) Lin, T.-C.; Huang, B.-R. Palladium Nanoparticles Modified Carbon Nanotube/Nickel Composite Rods (Pd/CNT/Ni) for Hydrogen Sensing. *Sens. Actuators, B* **2012**, *162*, 108−113.

(7) Petta, J. R.; Slater, S. K.; Ralph, D. C. Spin-Dependent Transport in Molecular Tunnel Junctions. *Phys. Rev. Lett.* **2004**, *93*, 136601-1−136601-4.

(8) Corbierre, M. K.; Lennox, R. B. Preparation of Thiol-Capped Gold Nanoparticles by Chemical Reduction of Soluble Au(I)−Thiolates. *Chem. Mater.* **2005**, *17*, 5691−5696.

(9) Barngrover, B. M.; Aikens, C. M. The Golden Pathway to Thiolate-Stabilized Nanoparticles: Following the Formation of Gold-(I) Thiolate from Gold(III) Chloride. *J. Am. Chem. Soc.* **2012**, *134*, 12590−12595.

(10) Hostetler, M. J.; Wingate, J. E.; Zhong, C.-J.; Harris, J. E.; Vachet, R. W.; Clark, M. R.; Londono, J. D.; Green, S. J.; Stokes, J. J.; Wignall, G. D.; Glish, G. L.; Porter, M. D.; Evans, N. D.; Murray, R. W. Alkanethiolate Gold Cluster Molecules with Core Diameters from 1.5 to 5.2 Nm: Core and Monolayer Properties as a Function of Core Size. *Langmuir* **1998**, *14*, 17−30.

(11) Goulet, P. J. G.; Lennox, R. B. New Insights into Brust−Schiffrin Metal Nanoparticle Synthesis. *J. Am. Chem. Soc.* **2010**, *132*, 9582−9584.

(12) Corthey, G.; Giovanetti, L. J.; Ramallo-López, J. M.; Zelaya, E.; Rubert, A. A.; Benitez, G. A.; Requejo, F. G.; Fonticelli, M. H.; Salvarezza, R. C. Synthesis and Characterization of Gold@Gold(I)−Thiomalate Core@Shell Nanoparticles. *ACS Nano* **2010**, *4*, 3413−3421.

(13) Leff, D. V.; Brandt, L.; Heath, J. R. Synthesis and Characterization of Hydrophobic, Organically-Soluble Gold Nanocrystals Functionalized with Primary Amines. *Langmuir* **1996**, *12*, 4723−4730.

(14) Eklund, S. E.; Cliffel, D. E. Synthesis and Catalytic Properties of Soluble Platinum Nanoparticles Protected by a Thiol Monolayer. *Langmuir* **2004**, *20*, 6012−6018.

(15) Chen, S.; Kimura, K. Synthesis of Thiolate-Stabilized Platinum Nanoparticles in Protolytic Solvents as Isolable Colloids. *J. Phys. Chem. B* **2001**, *105*, 5397−5403.

(16) Zamborini, F. P.; Gross, S. M.; Murray, R. W. Synthesis, Characterization, Reactivity, and Electrochemistry of Palladium Monolayer Protected Clusters. *Langmuir* **2001**, *17*, 481−488.

(17) Ohyama, J.; Teramura, K.; Higuchi, Y.; Shishido, T.; Hitomi, Y.; Kato, K.; Tanida, H.; Uruga, T.; Tanaka, T. In Situ Observation of Nucleation and Growth Process of Gold Nanoparticles by Quick XAFS Spectroscopy. *ChemPhysChem* **2011**, *12*, 127−131.

(18) Wu, Z.; MacDonald, M. A.; Chen, J.; Zhang, P.; Jin, R. Kinetic Control and Thermodynamic Selection in the Synthesis of Atomically Precise Gold Nanoclusters. *J. Am. Chem. Soc.* **2011**, *133*, 9670−9673.

(19) Li, Y.; Zaluzhna, O.; Tong, Y. J. Critical Role of Water and the Structure of Inverse Micelles in the Brust−Schiffrin Synthesis of Metal Nanoparticles. *Langmuir* **2011**, *27*, 7366−7370.

(20) Li, Y.; Zaluzhna, O.; Zangmeister, C. D.; Allison, T. C.; Tong, Y. J. Different Mechanisms Govern the Two-Phase Brust−Schiffrin Dialkylditelluride Syntheses of Ag and Au Nanoparticles. *J. Am. Chem. Soc.* **2012**, *134*, 1990−1992.

(21) Corthey, G.; Rubert, A. A.; Picone, A. L.; Casillas, G.; Giovanetti, L. J.; Ramallo-López, J. M.; Zelaya, E.; Benitez, G. A.; Requejo, F. G.; José-Yacamán, M.; Salvarezza, R. C.; Fonticelli, M. H. New Insights into the Chemistry of Thiolate-Protected Palladium Nanoparticles. *J. Phys. Chem. C* **2012**, *116*, 9830−9837.

(22) Moreno, M.; Ibañez, F. J.; Jasinski, J. B.; Zamborini, F. P. Hydrogen Reactivity of Palladium Nanoparticles Coated with Mixed Monolayers of Alkyl Thiols and Alkyl Amines for Sensing and Catalysis Applications. *J. Am. Chem. Soc.* **2011**, *133*, 4389−4397.

(23) Peng, L.; Jianguo, G.; Qingjie, Z.; Wenyu, Z. Preparation and Characterization of Monodisperse Nickel Nanoparticles by Polyol Process. *J. Wuhan Univ. Technol.* **2005**, *20*, 35−37.

(24) Brust, M.; Kiely, C. J. Some Recent Advances in Nanostructure Preparation from Gold and Silver Particles: A Short Topical Review. *Colloids Surf., A* **2002**, *202*, 175−186.

(25) Ibañez, F. J.; Zamborini, F. P. Reactivity of Hydrogen with Solid-State Films of Alkylamine- and Tetraoctylammonium Bromide-Stabilized Pd, PdAg, and PdAu Nanoparticles for Sensing and Catalysis Applications. *J. Am. Chem. Soc.* **2008**, *130*, 622−633.

(26) Carro, P.; Corthey, G.; Rubert, A. A.; Benitez, G. A.; Fonticelli, M. H.; Salvarezza, R. C. The Complex Thiol−Palladium Interface: A

Theoretical and Experimental Study. *Langmuir* **2010**, *26*, 14655–14662.

(27) Eriksson, S.; Nylén, U.; Rojas, S.; Boutonnet, M. Preparation of Catalysts from Microemulsions and Their Applications in Heterogeneous Catalysis. *Appl. Catal., A* **2004**, *265*, 207–219.

(28) El-Gendy, A. A.; Ibrahim, E. M. M.; Khavrus, V. O.; Krupskaya, Y.; Hampel, S.; Leonhardt, A.; Büchner, B.; Klingeler, R. The Synthesis of Carbon Coated Fe, Co and Ni Nanoparticles and an Examination of Their Magnetic Properties. *Carbon* **2009**, *47*, 2821–2828.

(29) Knecht, M. R.; Garcia-Martinez, J. C.; Crooks, R. M. Synthesis, Characterization, and Magnetic Properties of Dendrimer-Encapsulated Nickel Nanoparticles Containing <150 Atoms. *Chem. Mater.* **2006**, *18*, 5039–5044.

(30) Mourdikoudis, S.; Simeonidis, K.; Vilalta-Clemente, A.; Tuna, F.; Tsiaoussis, I.; Angelakeris, M.; Dendrinou-Samara, C.; Kalogirou, O. Controlling the Crystal Structure of Ni Nanoparticles by the Use of Alkylamines. *J. Magn. Magn. Mater.* **2009**, *321*, 2723–2728.

(31) Bradley, J. S.; Tesche, B.; Busser, W.; Maase, M.; Reetz, M. T. Surface Spectroscopic Study of the Stabilization Mechanism for Shape-Selectively Synthesized Nanostructured Transition Metal Colloids. *J. Am. Chem. Soc.* **2000**, *122*, 4631–4636.

(32) Auten, B. J.; Hahn, B. P.; Vijayaraghavan, G.; Stevenson, K. J.; Chandler, B. D. Preparation and Characterization of 3 nm Magnetic NiAu Nanoparticles. *J. Phys. Chem. C* **2008**, *112*, 5365–5372.

(33) Malinga, S. P.; Arotiba, O. A.; Krause, R. W.; Mapolie, S. F.; Mamba, B. B. Synthesis and Characterization of Generation 2 and 3 Poly(propylene Imine) Dendrimer Capped NiFe Nanoalloy. *Mater. Lett.* **2012**, *68*, 324–326.

(34) Wu, L.; Ling, J.; Wu, Z.-Q. A Highly Active and Recyclable Catalyst: Phosphine Dendrimer-Stabilized Nickel Nanoparticles for the Suzuki Coupling Reaction. *Adv. Synth. Catal.* **2011**, *353*, 1452–1456.

(35) Cordente, N.; Respaud, M.; Senocq, F.; Casanove, M.-J. Amiens, C.; Chaudret, B. Synthesis and Magnetic Properties of Nickel Nanorods. *Nano Lett.* **2001**, *1*, 565–568.

(36) Legrand, J.; Taleb, A.; Gota, S.; Guittet, M.-J.; Petit, C. Synthesis and XPS Characterization of Nickel Boride Nanoparticles. *Langmuir* **2002**, *18*, 4131–4137.

(37) Glavee, G. N.; Klabunde, K. J.; Sorensen, C. M.; Hadjipanayis, G. C. Borohydride Reduction of Nickel and Copper Ions in Aqueous and Nonaqueous Media. Controllable Chemistry Leading to Nanoscale Metal and Metal Boride Particles. *Langmuir* **1994**, *10*, 4726–4730.

(38) Mekhalif, Z.; Delhalle, J.; Pireaux, J.-J.; Noël, S.; Houzé, F.; Boyer, L. Surface Modifications of Nickel Substrates with Self-Assembled Monolayers of Alkanethiols for Electrical Contact Applications. *Surf. Coat. Technol.* **1998**, *100–101*, 463–468.

(39) Bengió, S.; Fonticelli, M.; Benítez, G.; Creus, A. H.; Carro, P.; Ascolani, H.; Zampieri, G.; Blum, B.; Salvarezza, R. C. Electrochemical Self-Assembly of Alkanethiolate Molecules on Ni(111) and Polycrystalline Ni Surfaces. *J. Phys. Chem. B* **2005**, *109*, 23450–23460.

(40) Rajalingam, S.; Devillers, S.; Dehalle, J.; Mekhalif, Z. A Two Step Process to Form Organothiol Self-Assembled Monolayers on Nickel Surfaces. *Thin Solid Films* **2012**, *522*, 247–253.

(41) Sadler, J. E.; Szumski, D. S.; Kierzkowska, A.; Catarelli, S. R.; Stella, K.; Nichols, R. J.; Fonticelli, M. H.; Benitez, G.; Blum, B.; Salvarezza, R. C.; Schwarzacher, W. Surface Functionalization of Electro-Deposited Nickel. *Phys. Chem. Chem. Phys.* **2011**, *13*, 17987–17993.

(42) Lee, E.; Lee, J. M.; Koo, J. H.; Lee, W.; Lee, T. Hysteresis Behavior of Electrical Resistance in Pd Thin Films During the Process of Absorption and Desorption of Hydrogen Gas. *Int. J. Hydrogen Energy* **2010**, *35*, 6984–6991.

(43) Lee, E.; Lee, J. M.; Lee, E.; Noh, J.-S.; Joe, J. H.; Jung, B.; Lee, W. Hydrogen Gas Sensing Performance of Pd–Ni Alloy Thin Films. *Thin Solid Films* **2010**, *519*, 880–884.

(44) Park, J. B.; Jeong, S. H.; Jeong, M. S.; Kim, J. Y.; Cho, B. K. Synthesis of Carbon-Encapsulated Magnetic Nanoparticles by Pulsed Laser Irradiation of Solution. *Carbon* **2008**, *46*, 1369–1377.

(45) Latham, A. H.; Williams, M. E. Transmission Electron Microscope-Induced Structural Evolution in Amorphous Fe, Co, and Ni Oxide Nanoparticles. *Langmuir* **2008**, *24*, 14195–14202.

(46) Dalfovo, M. C.; Salvarezza, R. C.; Ibañez, F. J. Improved Vapor Selectivity and Stability of Localized Surface Plasmon Resonance with a Surfactant-Coated Au Nanoparticles Film. *Anal. Chem.* **2012**, *84*, 4886–4892.

(47) Hostetler, M. J.; Stokes, J. J.; Murray, R. W. Infrared Spectroscopy of Three-Dimensional Self-Assembled Monolayers: N-Alkanethiolate Monolayers on Gold Cluster Compounds. *Langmuir* **1996**, *12*, 3604–3612.

(48) 1-Dodecanethiol. http://webbook.nist.gov/cgi/cbook.cgi?Name=1-Dodecanethiol&Units=SI&cIR=on&cUV=on#IR-Spec, accessed Sept 13, 2012.

(49) John, N. S.; Kulkarni, G. U.; Datta, A.; Pati, S. K.; Komori, F.; Kavitha, G.; Narayana, C.; Sanyal, M. K. Magnetic Interactions in Layered Nickel Alkanethiolates. *J. Phys. Chem. C* **2007**, *111*, 1868–1870.

(50) John, N. S.; Thomas, P. J.; Kulkarni, G. U. Self-Assembled Hybrid Bilayers of Palladium Alkanethiolates. *J. Phys. Chem. B* **2003**, *107*, 11376–11381.

(51) Chen, S.; Kimura, K. Synthesis and Characterization of Carboxylate-Modified Gold Nanoparticle Powders Dispersible in Water. *Langmuir* **1999**, *15*, 1075–1082.

(52) Ristau, R.; Tiruvalam, R.; Clasen, P. L.; Gorskowski, E. P.; Harmer, M. P.; Kiely, C. J.; Hussain, I.; Brust, M. Electron Microscopy Studies of the Thermal Stability of Gold Nanoparticle Arrays. *Gold Bull.* **2009**, *42*, 133–143.

(53) Radha, B.; Kiruthika, S.; Kulkarni, G. U. Metal Anion–Alkyl Ammonium Complexes as Direct Write Precursors to Produce Nanopatterns of Metals, Nitrides, Oxides, Sulfides, and Alloys. *J. Am. Chem. Soc.* **2011**, *133*, 12706–12713.

(54) Hwang, J.-H.; Dravid, V. P.; Teng, M. H.; Host, J. J.; Elliott, B. R.; Johnson, D. L.; Mason, T. O. Magnetic Properties of Graphitically Encapsulated Nickel Nanocrystals. *J. Mater. Res.* **1997**, *12*, 1076–1082.

(55) Chen, D.-H.; Wu, S.-H. Synthesis of Nickel Nanoparticles in Water-in-Oil Microemulsions. *Chem. Mater.* **2000**, *12*, 1354–1360.

(56) Sandhyarani, N.; Pradeep, T. An Investigation of the Structure and Properties of Layered Copper Thiolates. *J. Mater. Chem.* **2001**, *11*, 1294–1299.

(57) Parikh, A. N.; Gillmor, S. D.; Beers, J. D.; Beardmore, K. M.; Cutts, R. W.; Swanson, B. I. Characterization of Chain Molecular Assemblies in Long-Chain, Layered Silver Thiolates: A Joint Infrared Spectroscopy and X-ray Diffraction Study. *J. Phys. Chem. B* **1999**, *103*, 2850–2861.

(58) Yang, Z.; Smetana, A. B.; Sorensen, C. M.; Klabunde, K. J. Synthesis and Characterization of a New Tiara Pd(II) Thiolate Complex, $[Pd(SC_{12}H_{25})_2]_6$, and Its Solution-Phase Thermolysis to Prepare Nearly Monodisperse Palladium Sulfide Nanoparticles. *Inorg. Chem.* **2007**, *46*, 2427–2431.

(59) Datta, A.; John, N. S.; Kulkarni, G. U.; Pati, S. K. Aromaticity in Stable Tiara Nickel Thiolates: Computational and Structural Analysis. *J. Phys. Chem. A* **2005**, *109*, 11647–11649.

(60) Lin, X.; Burns, R. C.; Lawrance, G. A. Effect of Electrolyte Composition, and of Added Iron(III) in the Presence of Selected Organic Complexing Agents, on Nickel(II) Precipitation by Lime. *Water Res.* **1998**, *32*, 3637–3645.